Supporting Information for:

A More Reactive Trigonal Bipyramidal High-Spin Oxoiron(IV) Complex with a *cis*-Labile Site.

Jason England, Yisong Guo, Katherine M. Van Heuvelen, Matthew A. Cranswick, Gregory T. Rohde, Emile L. Bominaar,* Eckard Münck,* and Lawrence Que, Jr.*

Contents:

Materials and Instrumentation.

All reagents were purchased from vendors and used as received, unless noted otherwise. Diethyl ether and tetrahydrofuran were dried by prolonged reflux, under a nitrogen atmosphere, over sodium metal with a benzophenone ketyl indicator and distilled freshly prior to use. Acetonitrile and dichloromethane were treated in a similar manner, but using calcium hydride as the drying agent. The reagents 2-(*tert*-butylsulfonyl)iodosylbenzene (2-(^{t}BuSO$_2$)C$_6$H$_4$IO),[1] Fe(OTf)$_2$(CH$_3$CN)$_2$[2] and chlorotetramethylformamidinium chloride ([(Me$_2$N)$_2$CCl]Cl)[3] were all prepared according to published procedures.

All moisture and oxygen sensitive compounds were prepared using a standard high vacuum line and Schlenk techniques. A nitrogen-filled glove box was used for any subsequent manipulation and storage of these compounds. ^{1}H, ^{13}C and ^{19}F (+150 to -200 ppm) NMR spectra were recorded on a Varian Inova 500 MHz spectrometer at ambient temperature. Chemical shifts (ppm) were referenced to the residual protic solvent peaks. Elemental analyses for **2** were performed by Atlantic Microlab (Norcross, GA). UV-Visible studies were performed using a HP8453A diode array spectrometer equipped with a cryostat from Unisoku Scientific Instruments (Osaka, Japan). Electrospray ionization mass spectrometry experiments were carried out on a Bruker BioTOF II mass spectrometer using a spray chamber voltage of 4000 V and a gas carrier temperature of 60ºC.

Mössbauer spectra were recorded with two spectrometers, using Janis Research Super-Varitemp dewars that allowed studies in applied magnetic fields up to 8.0 T in temperature range from 1.5 to 200 K. Mössbauer spectral simulations were performed using the WMOSS software package (SEE Co, Edina, MN). Isomer shifts are quoted relative to Fe metal at 298 K.

Parallel-mode X band (9.28 GHz) EPR spectra were recorded on a Bruker ESR 300 spectrometer equipped with an Oxford ESR 910 liquid Helium cryostat and an Oxford temperature controller. The microwave frequency was calibrated with a frequency counter and the magnetic field with a NMR gaussmeter. EPR spectral simulations were carried out using a Windows software package (SpinCount) available from Professor Michael Hendrich of Carnegie Mellon University. The simulations are least-squares fits of the experimental spectra.

Synthetic Procedures.

TMG_2dien [2',2'-(2,2'-(methylazanediyl)bis(ethane-1,2-diyl))bis(1,1,3,3-tetramethyl-guanidine]: this ligand was synthesized according to the general procedure outlined in reference 4, using 5.00 g (29.2 mmol) of $[(Me_2N)_2CCl]Cl$ and 1.71 g (14.6 mmol) of N^2-methyldiethylenetriamine. The product was obtained as a yellow oil (4.1 g, 90 %). ^{1}H-NMR ($CDCl_3$, 500 MHz): δ 3.27 (m, 4 H, CH_2), 2.73 (s, 12 H, NMe_2), 2.62 (s, 12 H, NMe_2), 2.58 (m, 4 H, CH_2), 2.33 (s, 3 H, NCH_3). ^{13}C-NMR ($CDCl_3$, 125 MHz): δ 160.4 (N=C), 61.1 (NCH_3), 48.4 (CH_2), 43.7 (CH_2), 39.6 (NMe_2), 38.8 (NMe_2). MS (+ESI): *m/z* 314.3 $[(M+H)^+]$.

$[Fe^{II}(TMG_2dien)(Cl)_2]$ (**5**): A mixture of TMG_2dien (0.30 g, 0.96 mmol) and iron(II) dichloride (0.12 g, 0.96 mmol) was stirred in tetrahydrofuran (10 mL) for 12 hours, during which time a precipitate formed. This solid was isolated by filtration, washed with tetrahydrofuran (5 mL) and diethyl ether (15 mL), and dried under vacuum to give the product as a white powder (0.40 g, 95 %). Crystals suitable for X-ray analysis were obtained by vapor diffusion of diethyl ether into a concentrated dichloromethane solution of the complex. ^{1}H-NMR (CD_3CN, all peaks appear as broad singlets): δ 80.6 (3 H, NCH_3), 23.1 (24 H, NMe_2). MS (+ESI): *m/z* 404.2 $[(M-Cl)^+]$. Anal. Calcd. (found) for $C_{15}H_{35}Cl_2FeN_7$: C, 40.92 (40.83); H, 8.01 (8.03); N, 22.27 (22.32).

$[Fe^{II}(TMG_2dien)(OTf)_2]$ (**4**): A mixture of **5** (0.20 g, 0.45 mmol) and thallium(I) triflate (0.32 g, 0.91 mmol) was stirred in dichloromethane (10 mL) for 18 hours. The resultant mixture was filtered to remove thallium(I) salts and the filtrate was reduced to dryness, thereby yielding the product as an off-white to cream colored solid (0.29 g, 96 %). Crystals suitable for X-ray analysis were obtained by vapor diffusion of diethyl ether into a concentrated dichloromethane solution of the complex. ^{1}H-NMR (CD_3CN, all peaks appear as broad singlets): δ 178.1 (1 H, CH_2), 159.9 (1 H, CH_2), 156.0 (1 H, CH_2), 116.1 (3 H, NMe), 97.7 (1 H, CH_2), 66.6 (1 H, CH_2), 57.5 (1 H, CH_2), 38.4 (6 H, NMe_2), 35.4 (3 H, NMe_2), 33.3 (3 H, NMe_2), 30.7 (3 H, NMe_2), 21.5 (7 H, 2 NMe_2 + CH_2), 14.6 (1 H, CH_2), -36.5 (3 H, NMe_2). ^{19}F-NMR (CD_3CN, all peaks appear as broad singlets): δ -77.9. ^{19}F-NMR (CD_2Cl_2, all peaks appear as broad singlets): δ -35. MS (+ESI): *m/z* 518.2 $[(M-OTf)^+]$, 184.6 $[\{M-(OTf)_2\}^{2+}]$. Anal. Calcd. (found) for $C_{17}H_{35}F_6FeN_7O_6S_2.2H_2O$: C, 29.02 (29.23); H, 5.59 (5.57); N, 13.94 (13.87).

$[Fe^{IV}(O)(TMG_2dien)(CH_3CN)]^{2+}$ (**7**): Solutions of the orange-brown complex **7** were prepared by reaction of acetonitrile solutions of **4** with three equivalents of 2-(^{t}BuSO$_2$)C_6H_4IO,

dissolved in dichloromethane. Solutions of oxidant up to a concentration of 80 mM were routinely used.

$[Fe^{IV}(O)(TMG_2dien)(X)]^+$ (**7-X**, X = N_3, Cl): Solutions of the anion substituted complexes **7-N_3** and **7-Cl** were prepared from **7** by the addition of ≥ 2 equivalents of acetonitrile solutions of tetrabutylammonium azide and tetrabutylammonium/ tetraheptylammonium chloride, respectively.

X-Ray Crystallography.

Selected single crystals of **4** and **5** were placed onto the top of 0.1 mm diameter glass capillaries and mounted on a Bruker SMART V5.054 CCD area detector diffractometer for data collection at temperatures of 173(2) and 123(2) K, respectively. A preliminary set of cell constants was collected from reflections harvested from three sets of 20 frames. These initial sets of frames were oriented such that orthogonal wedges of reciprocal space were surveyed and then used to produce initial orientation matrices. Data collection was carried out using MoKα radiation (graphite monochromator), with a detector distance of 4.8 cm and frame times of 30 and 15 seconds for **4** and **5**, respectively. A randomly oriented region of reciprocal space was surveyed to the extent of one sphere and to a resolution of 0.77 Å, with four major sections of frames being collected using 0.30° steps in ω at four different ϕ settings and a detector position of -28° in 2θ. The intensity data were corrected for absorption and decay (SADABS).[5] Final cell constants were calculated from the actual data collection after integration (SAINT).[6] Please refer to Tables S1 and S2, plus accompanying text, for additional crystal and refinement information.

The structures were solved and refined using Bruker SHELXTL.[7] Space groups were determined based on systematic absences and intensity statistics. In both cases a direct-methods solution was calculated, which provided most non-hydrogen atoms from the E-map. The remaining non-hydrogen atoms were located by full-matrix least squares/ difference Fourier cycles. All non-hydrogen atoms were refined with anisotropic displacement parameters. All hydrogen atoms were placed in ideal positions and refined as riding atoms with relative isotropic displacement parameters.

Table S1. Crystal data and structure refinement for $[Fe^{II}(TMG_2dien)(OTf)_2]$ (**4**).

Identification code	09197a	
Empirical formula	$C_{17}\ H_{35}\ F_6\ Fe\ N_7\ O_6\ S_2$	
Formula weight	667.49	
Temperature	173(2) K	
Wavelength	0.71073 Å	
Crystal system	Monoclinic	
Space group	$P2_1/c$	
Unit cell dimensions	a = 18.512(3) Å	$\alpha = 90°$
	b = 9.1559(14) Å	$\beta = 106.291(2)°$
	c = 17.378(3) Å	$\gamma = 90°$
Volume	2827.2(7) $Å^3$	
Z	4	
Density (calculated)	1.568 Mg/m^3	
Absorption coefficient	0.766 mm^{-1}	
F(000)	1384	
Crystal color, morphology	Colorless, Needle	
Crystal size	0.50 x 0.22 x 0.20 mm^3	
Theta range for data collection	2.29 to 27.53°	
Index ranges	$-23 \le h \le 23, 0 \le k \le 11, 0 \le l \le 22$	
Reflections collected	26830	
Independent reflections	6456 [R(int) = 0.0405]	
Observed reflections	5063	
Completeness to theta = 27.53°	99.1%	
Absorption correction	Multi-scan	
Max. and min. transmission	0.858 and 0.817	
Refinement method	Full-matrix least-squares on F^2	
Data / restraints / parameters	6456 / 0 / 361	
Goodness-of-fit on F^2	1.014	
Final R indices [I>2sigma(I)]	$R1$ = 0.0379, $wR2$ = 0.0732	
R indices (all data)	$R1$ = 0.0581, $wR2$ = 0.0798	
Largest diff. peak and hole	0.334 and -0.426 $e.Å^{-3}$	

Table S2. Crystal data and structure refinement for $[Fe^{II}(TMG_2dien)(Cl)_2]$ (**5**).

Identification code	10016a	
Empirical formula	$C_{15}\ H_{35}\ Cl_2\ Fe\ N_7$	
Formula weight	440.25	
Temperature	123(2) K	
Wavelength	0.71073 Å	
Crystal system	Triclinic	
Space group	P-1	
Unit cell dimensions	a = 9.0439(11) Å	α = 68.485(2)°
	b = 10.4536(13) Å	β = 84.128(2)°
	c = 12.3764(16) Å	γ = 77.745(2)°
Volume	1063.4(2) $Å^3$	
Z	2	
Density (calculated)	1.375 Mg/m^3	
Absorption coefficient	0.974 mm^{-1}	
F(000)	468	
Crystal color, morphology	Colorless, Block	
Crystal size	0.40 x 0.32 x 0.26 mm^3	
Theta range for data collection	1.77 to 27.54°	
Index ranges	$-11 \le h \le 11, -12 \le k \le 13, 0 \le l \le 16$	
Reflections collected	12761	
Independent reflections	4808 [R(int) = 0.0262]	
Observed reflections	4224	
Completeness to theta = 27.54°	98.3%	
Absorption correction	Multi-scan	
Max. and min. transmission	0.91 and 0.84	
Refinement method	Full-matrix least-squares on F^2	
Data / restraints / parameters	4808 / 0 / 235	
Goodness-of-fit on F^2	1.041	
Final R indices [I>2sigma(I)]	$R1$ = 0.0259, $wR2$ = 0.0651	
R indices (all data)	$R1$ = 0.0318, $wR2$ = 0.0683	
Largest diff. peak and hole	0.344 and -0.215 $e.Å^{-3}$	

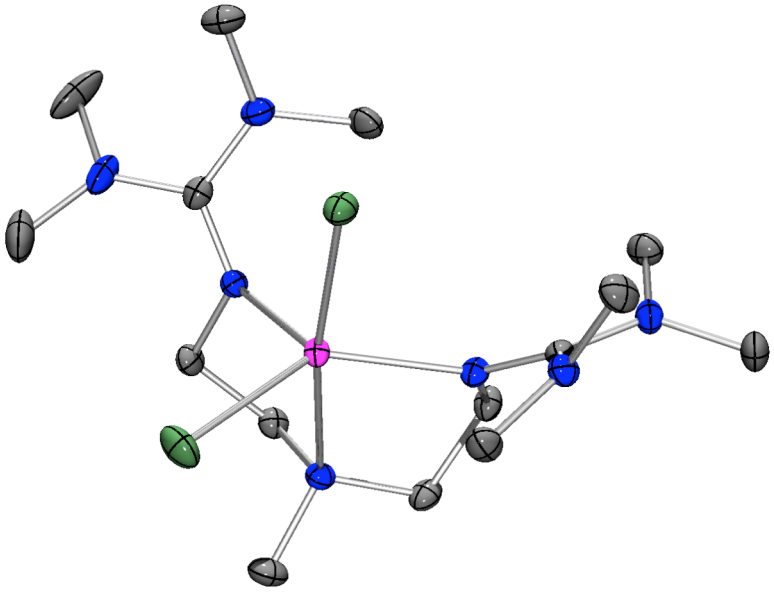

Figure S1. Thermal ellipsoid drawing of [$Fe^{II}(TMG_2dien)(Cl)_2$] (**5**), showing 50% probability ellipsoids. Hydrogen atoms have been omitted for clarity. Selected bond distances (Å): Fe-Cl_{axial}, 2.4370(5); Fe-$Cl_{equatorial}$, 2.3487(5); Fe-N_{axial}, 2.4187(12); Fe-$N_{guanidine}$(ave), 2.1096(12). Atom color scheme: C, gray; Cl, green; Fe, magenta; N, blue.

Reaction of $[Fe^{II}(TMG_2dien)(OTf)_2]$ (4) with Equimolar 2-($^tBuSO_2$)C_6H_4IO.

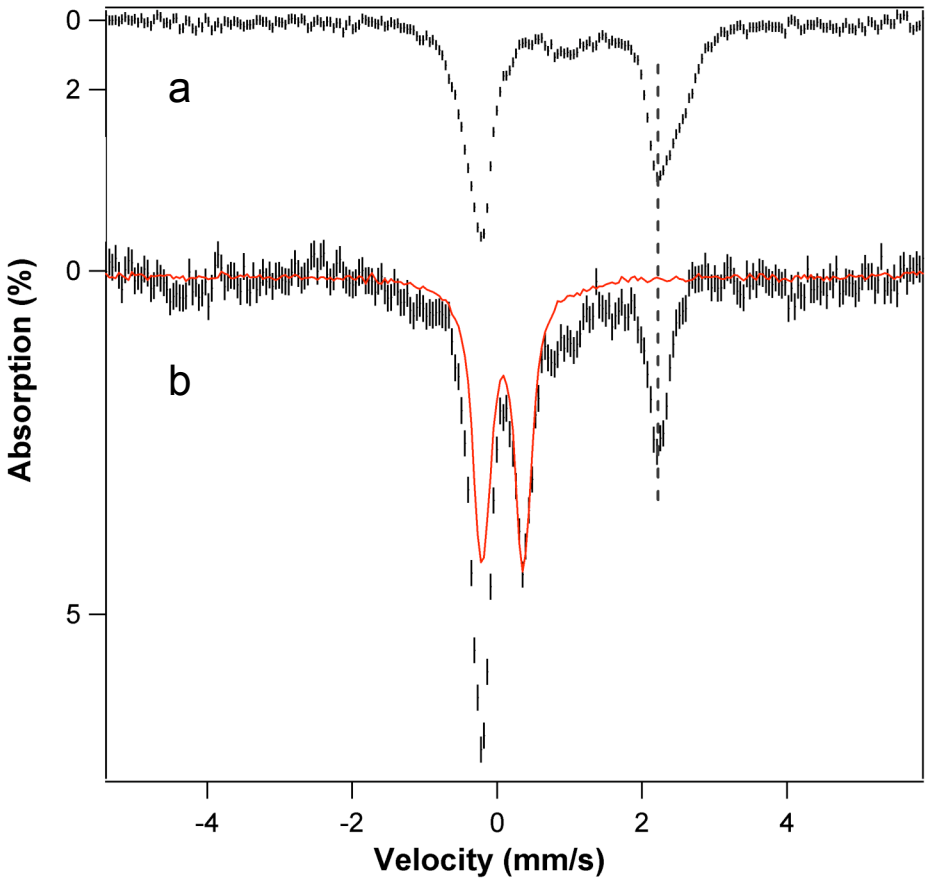

Figure S2. 4.2 K 0.45 kG Mössbauer spectra of (a) $[Fe^{II}(TMG_2dien)(OTf)_2]$ in CH_3CN, (b) the reaction product of $[Fe^{II}(TMG_2dien)(OTf)_2]$ with 1 equiv (black) and 3 equiv (red) of 2-($^tBuSO_2$)C_6H_4IO in CH_3CN. The intensity of the red curve was scaled to match the features of the spectrum in black hatched marks.

Resonance Raman Spectroscopy

Resonance Raman spectra were collected using a Spectra-Physics Model 2030-15 argon ion laser and an ACTON AM-506 monochromator equipped with a Princeton LN/CCD data collection system. Low temperature spectra in CH_3CN, CD_3CN, or 3:1 CH_3CN/CH_2Cl_2 were obtained at 77 K using a 135° backscattering geometry. Samples were frozen onto a gold-plated copper cold finger in thermal contact with a Dewar flask containing liquid nitrogen. Raman frequencies were calibrated to indene prior to data collection. The monochromator slit width was set for a band-pass of 4 cm^{-1} for all spectra. All spectra were collected with a laser excitation wavelength and power of 514.5 nm and 10 mW. Due to the photosensitivity of the samples the plotted spectra are the average of 3-5 spectra, which in turn are an average of 8 scans with collection times of 30 s. All spectra were intensity corrected to the 751 cm^{-1} solvent peak of CH_2Cl_2.

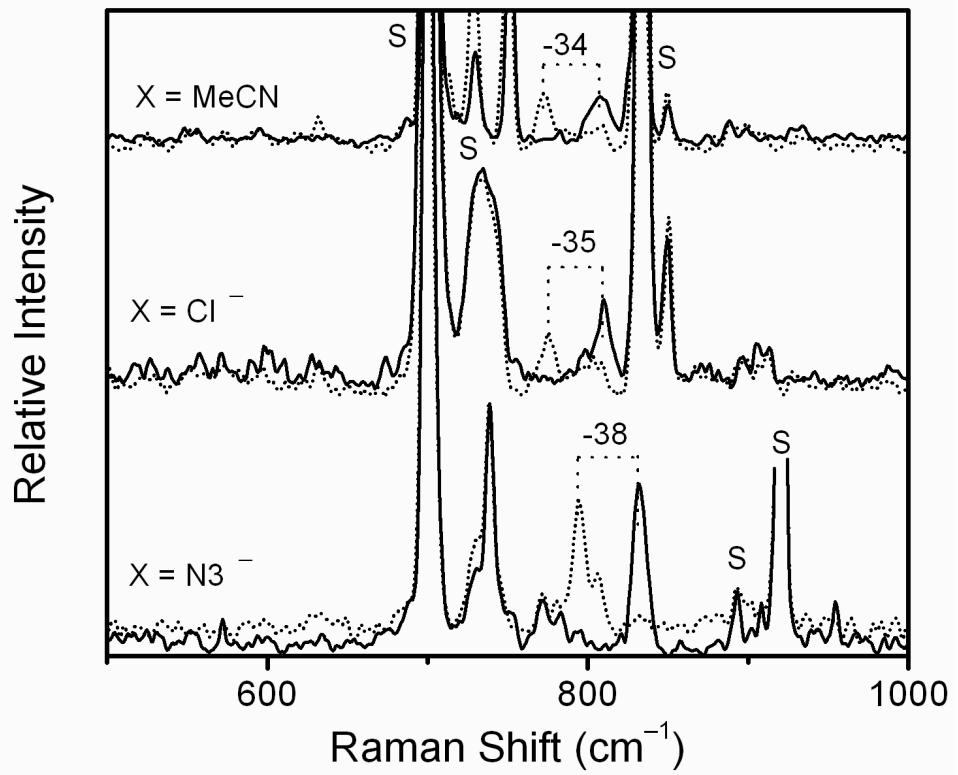

Figure S3. Resonance Raman spectra of $[Fe^{IV}(O)(TMGdien)(X)]^{2+/1+}$ where X = MeCN, Cl^-, and N_3^- (^{16}O – solid line; ^{18}O – dotted line) recorded with an excitation wavelength and power of 514.5 nm and 10 mW. Major solvent peaks are marked with an "S".

Comment on the Mössbauer parameters listed in Table 1.

The spectra were analyzed with the S = 2 spin Hamiltonian

$$\mathcal{H}_e = \mathrm{D}\left[\hat{S}_z^2 - 2 + (\mathrm{E/D})\left(\hat{S}_x^2 - \hat{S}_y^2\right)\right] + 2\beta\hat{\boldsymbol{S}}\cdot\boldsymbol{B} + \hat{\boldsymbol{S}}\cdot\ddot{\mathbf{A}}\cdot\hat{\boldsymbol{I}} - g_n\beta_n\boldsymbol{B}\cdot\hat{\boldsymbol{I}} + \mathcal{H}_Q$$

$$\mathcal{H}_Q = \left(eQV_{z'z'}/12\right)\left[3I_{z'}^2 - 15/14 + \eta\left(I_{x'}^2 - I_{y'}^2\right)\right]$$

(x',y',z') is the principal axis system of the EFG tensor; in WMOSS the Euler angles $[\alpha, \beta, \gamma]_{EFG}$ rotate (x', y', z') into the frame (x,y,z) of the zero-field splitting (ZFS) tensor. $\eta = (V_{x'x'}-V_{y'y'})/V_{z'z'}$ is the asymmetry parameter.

For our analysis we were confined to spectra recorded at 4.2 K. Above 10 K the applied field spectra spectra were unresolved due to intermediate relaxation of the electronic spin system. The listed (ZFS) parameters are quite good. E/D was obtained by EPR and the magnitude of D (ca. ± 0.5 cm^{-1}) follows from the field dependence of the magnetic hyperfine interactions. For **7** and **7-N_3** the uncertainties the x and y of the components of the ^{57}Fe magnetic hyperfine tensor are about ± 0.8 T. The electric field gradient (EFG) tensors of **7** and **7-N_3** we found to be rotated relative to the frame of the zero-field splitting tensor. As ΔE_Q is quite small, DFT calculations are not a reliable source of information about the EFG. Despite the fact that ΔE_Q is small, the analysis of the Mössbauer spectra indicates that the EFG tensors of **7** and **7-N_3** are rotated relative to the frame of the ZFS tensor as the EFG affects quite sensitively the positions of the absorption lines. Thus, because the electronic system is nearly axial and D > 0, the expectation values of the electronic spin are large in the xy plane and small along z. Consequently, the magnetic hyperfine field is large in the xy plane. Hence the Mössbauer spectra are mainly probing the components of the EFG in the xy plane. If the EFG is not rotated in the simulations the positions of the two inner lines of the magnetic spectra are not properly positioned relative to the outer lines. β_{EFG} is probably correct within 10°. For **7** and **7-N_3** the asymmetry parameter η is quite soft and difficult to determine with precision from the available data.

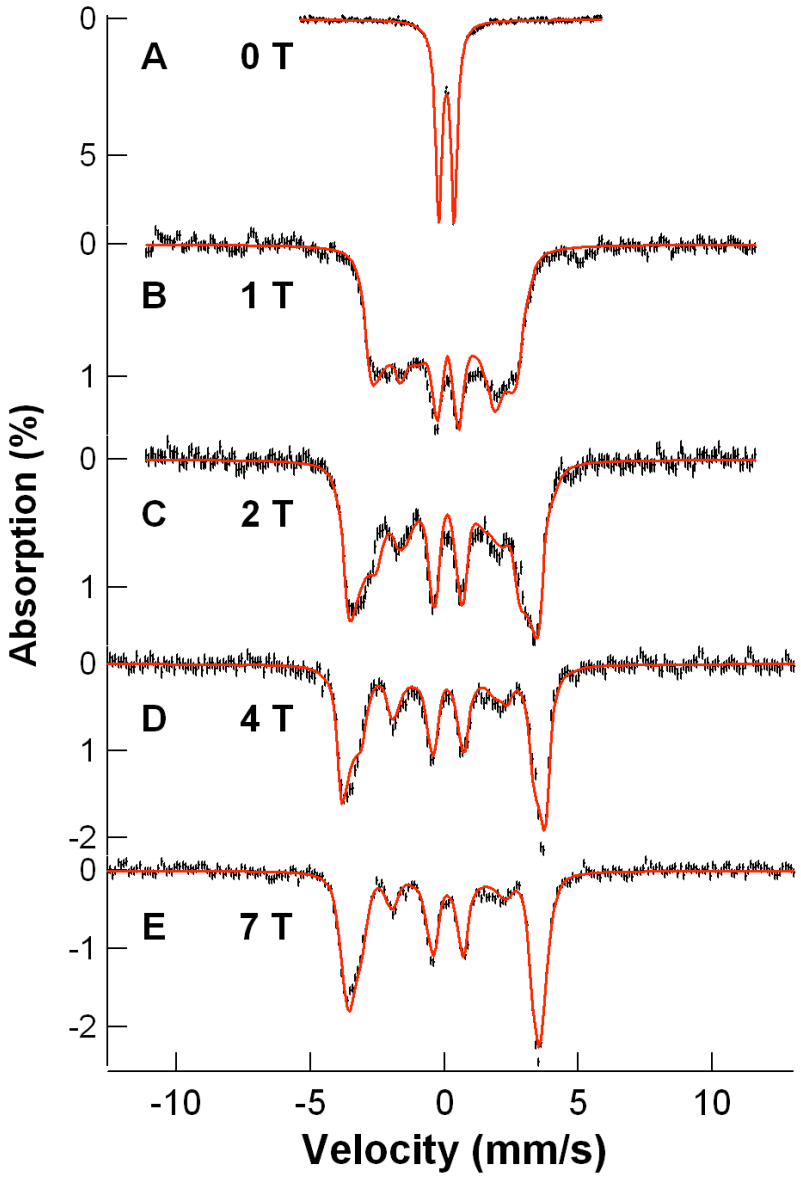

Figure S4. 4.2 K Mössbauer spectra of **7** in CH_3CN recorded in parallel applied magnetic fields as indicated. In all spectra, a high-spin Fe^{III} impurity, representing ~ 12% of the iron, has been subtracted from the raw data except for **A**. Solid lines are spectral simulations using the parameters listed in Table 1 in the main text.

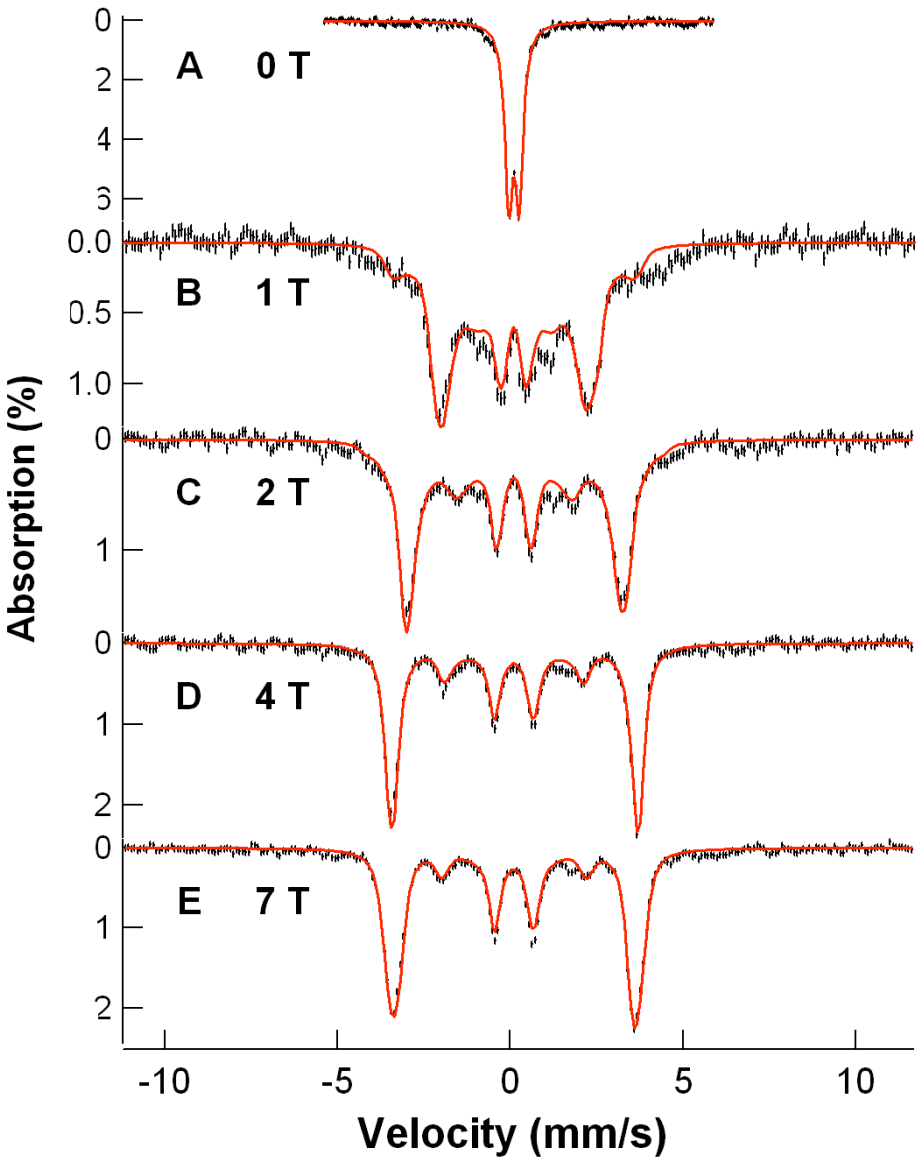

Figure S5. 4.2 K Mössbauer spectra of **7-N_3** in CH_3CN recorded in parallel applied magnetic fields as indicated. In all spectra, a high-spin Fe^{III} impurity, representing ~ 15% of the iron, has been subtracted from the raw data except for **A**. Solid lines are spectral simulations using the parameters listed in Table 1 in the main text.

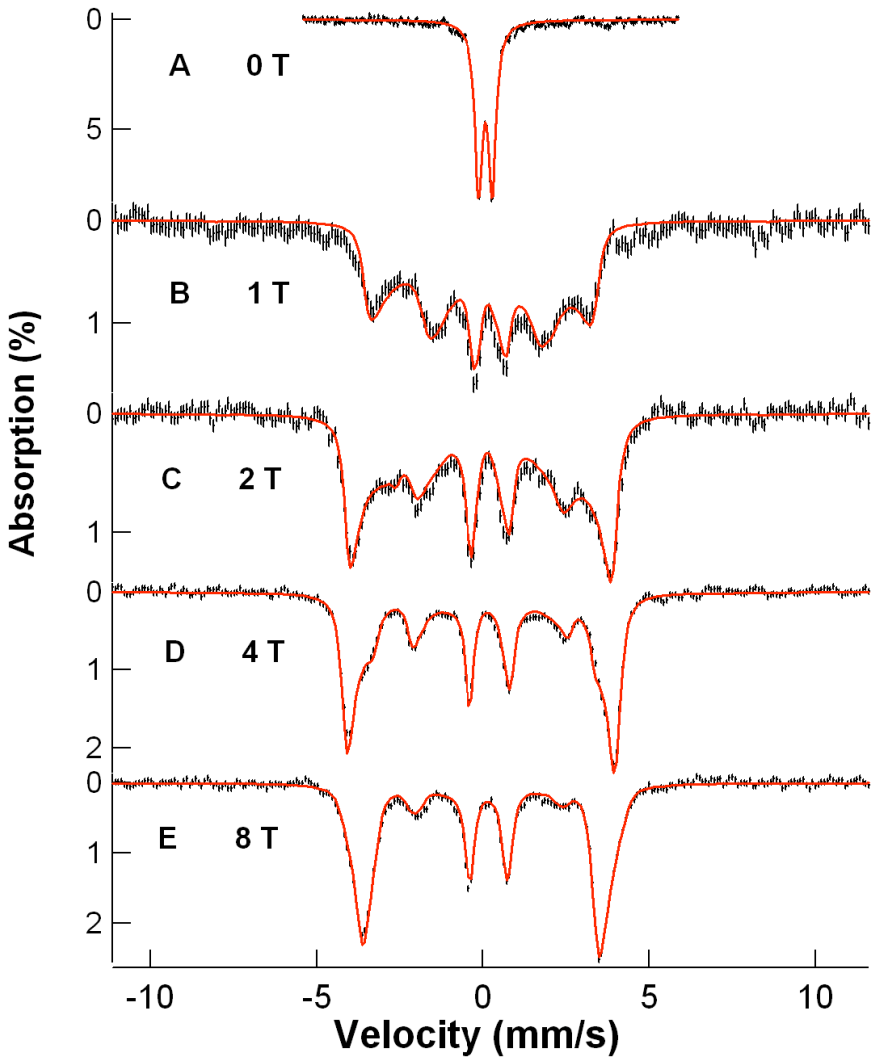

Figure S6. 4.2 K Mössbauer spectra of **7-Cl** in CH_3CN recorded in parallel applied magnetic fields as indicated. In all spectra, a high-spin Fe^{III} impurity, representing ~ 13% of the iron, has been subtracted from the raw data except for **A** and **B**. Solid lines are spectral simulations using the parameters listed in Table 1 in the main text.

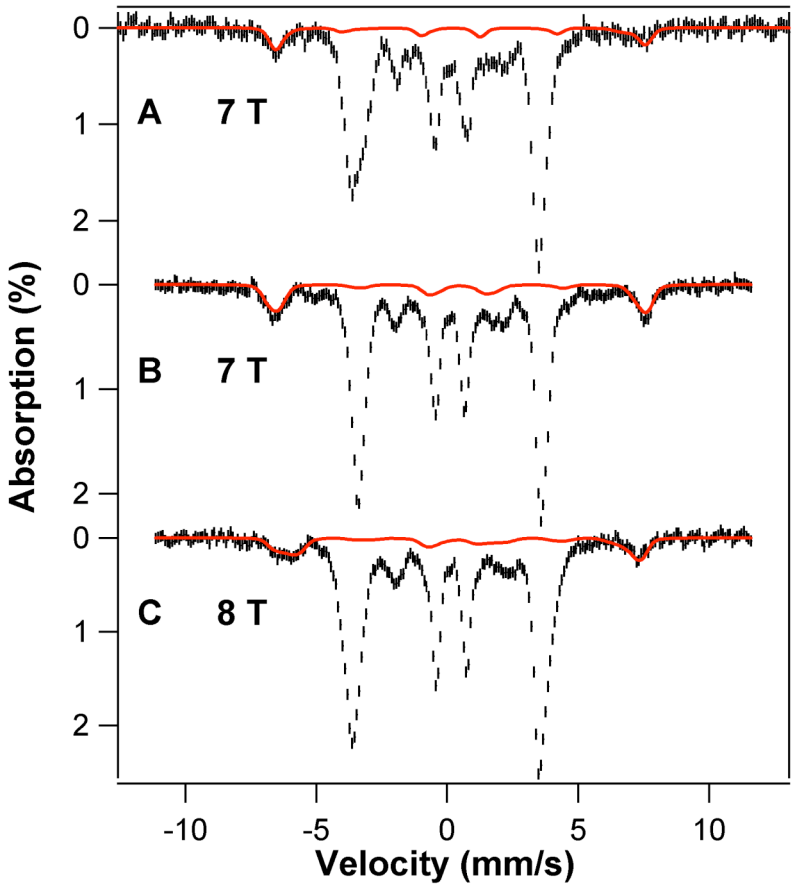

Figure S7. 4.2 K Mössbauer spectra of (A) **7**, (B) **7-N_3**, and (C) **7-Cl** in CH_3CN recorded in parallel applied magnetic fields as indicated (black). The red lines are spectral simulations indicating the high-spin Fe^{III} impurity in the samples (~12% for **7**, ~15% for **7-N_3**, and ~13% for **7-Cl**).

Additional EPR Spectra.

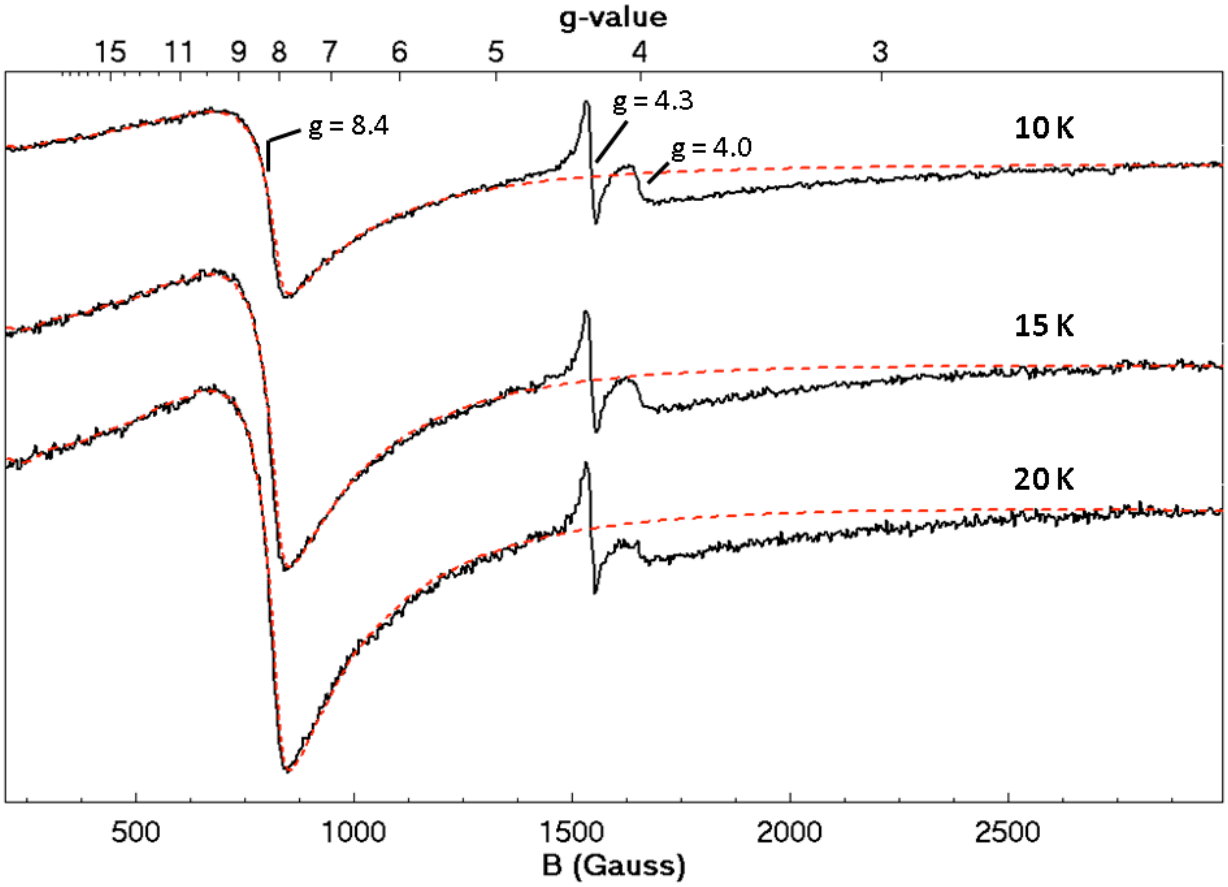

Figure S8. X band EPR spectra of **7** in CH_3CN (black) recorded at different temperatures as indicated. Red lines are SpinCount simulations for D = 4.2 cm^{-1}, E/D = 0.10, and σ(E/D) = 0.03. Experimental conditions: B1 || B, microwave power, 2 mW at 9.28 GHz. The signal at g = 4.3 is from the iron impurity, the signal at g = 4 is from trapped O_2 in the sample.

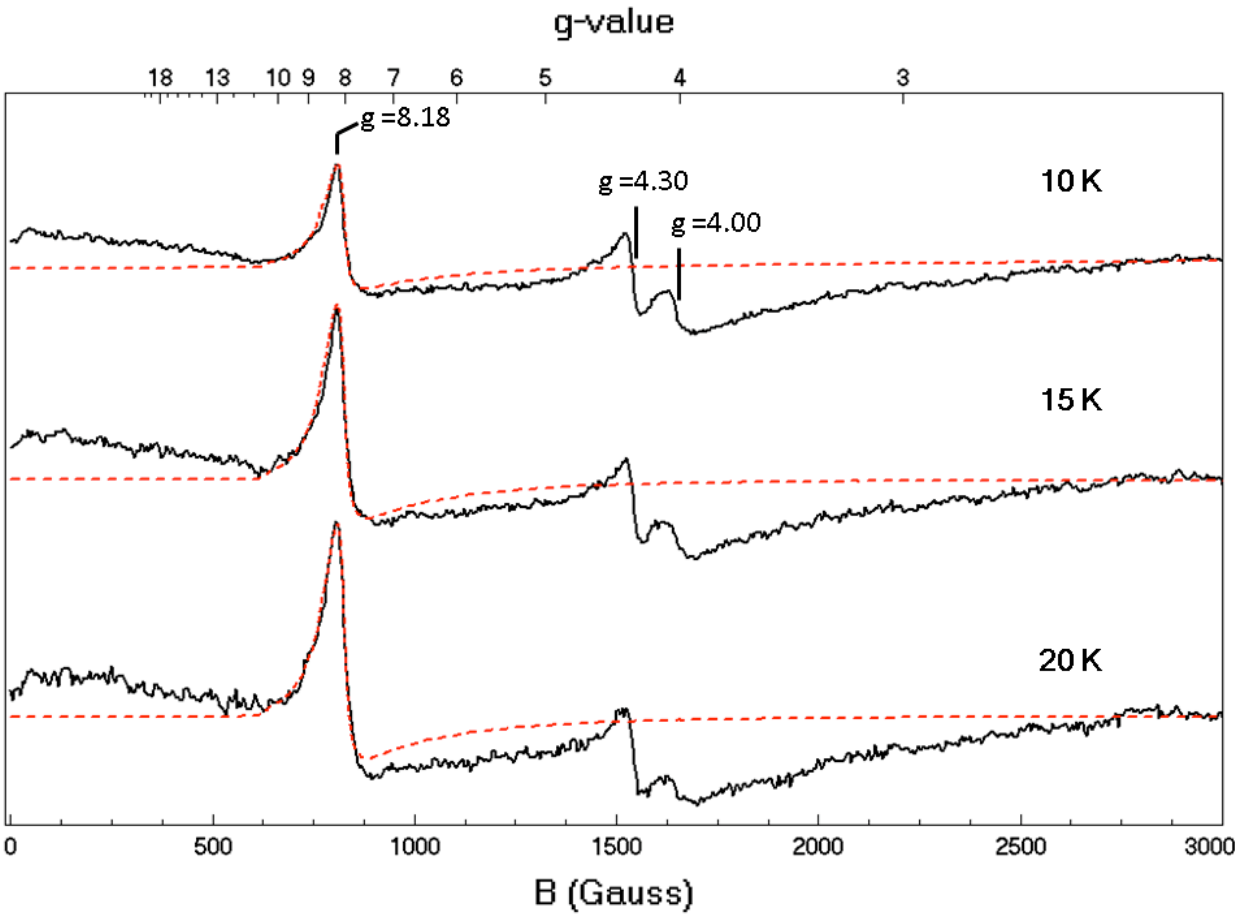

Figure S9. X band EPR spectra of **7-N_3** in CH_3CN (black) recorded at different temperatures as indicated. Red lines are SpinCount simulations for D = 5.0 cm^{-1}, E/D = 0.05, and σ(E/D) = 0.02. Experimental conditions: B1 || B, microwave power, 20 mW at 9.28 GHz. The signal at g = 4.3 is from the iron impurity, the signal at g = 4 is from trapped O_2 in the sample.

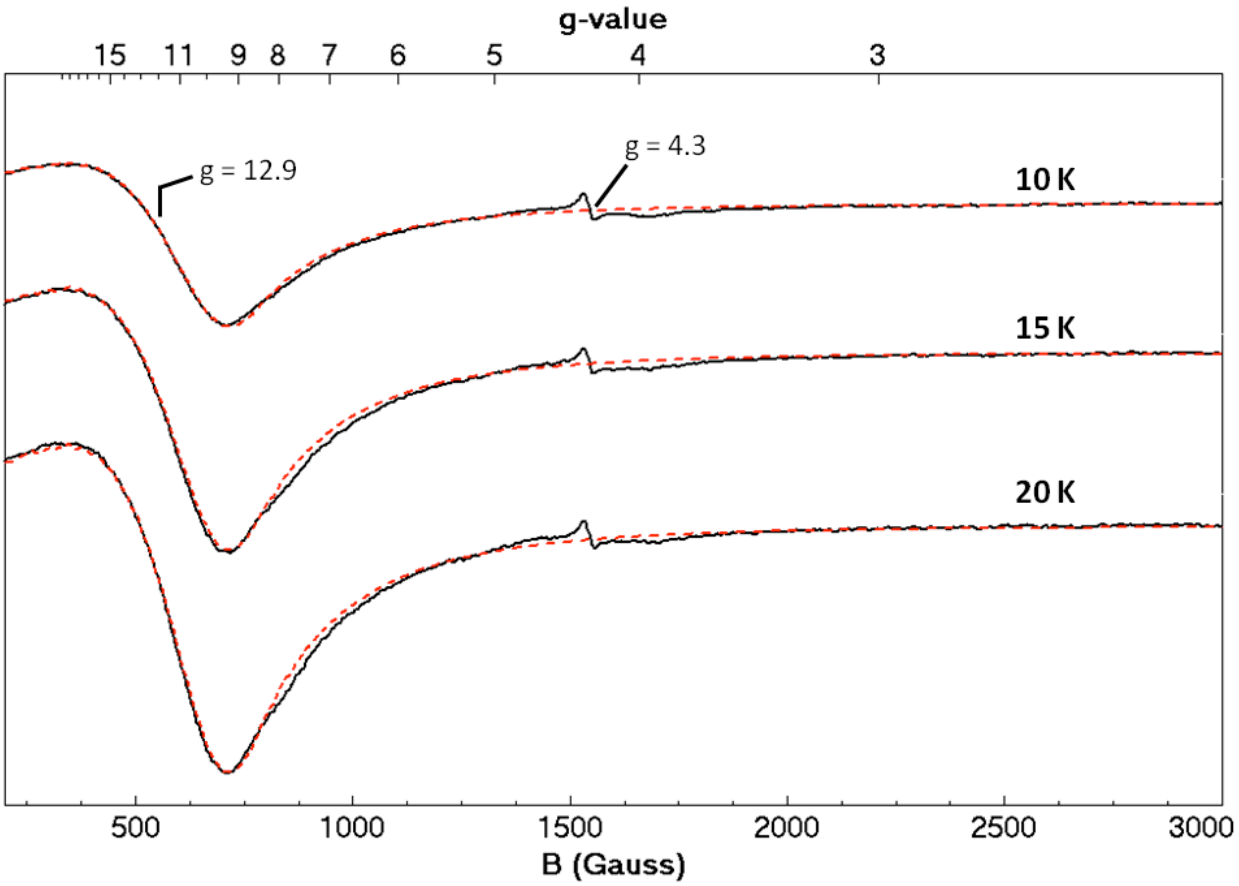

Figure S10. X band EPR spectra of **7-Cl** in CH_3CN (black) recorded at different temperatures as indicated. Red lines are SpinCount simulations for D = 4.2 cm^{-1}, E/D = 0.14, and σ(E/D) = 0.016. Experimental conditions: B1 || B, microwave power, 2 mW at 9.28 GHz. The signal at g = 4.3 is from the iron impurity.

XAS Studies.

X-ray absorption spectroscopic (XAS) data for **4**, **7**, **7-N_3**, and **7-Cl** were collected at the Stanford Synchrotron Radiation Lightsource (SSRL) of SLAC National Laboratory on the unfocussed beamline 7-3. Fe K-edge XAS data were collected over a range of 6.88 – 7.99 keV for frozen samples prepared in tandem Mössbauer/XAS cups in a mixture of acetonitrile/15% dichloromethane V/V (**4**, 5.1 mM; **7**, 5.0 mM, 82% Fe^{IV}; **7-N_3**, 5.1 mM, 85% Fe^{IV}; **7-Cl**, 5.0 mM, 78% Fe^{IV}). A Rh-coated harmonic rejection mirror was positioned upstream of the Si(220) double crystal monochromator. An Oxford Instruments CF1208 continuous flow liquid helium cryostat maintained a temperature of ~ 10 K in the sample compartment. Fluorescence data were collected with a 30 element solid-state germanium detector array (Canberra). An iron foil, run concurrently with the sample, was used for internal energy calibration, and the first inflection point of the Fe K-edge spectrum was taken to be 7112.0 eV.

Careful monitoring of the edge energy and the intensity of the pre-edge feature indicated that samples of **7** and **7-Cl** were somewhat susceptible to photoreduction. Such effects were minimized by realigning the sample to expose a new spot after collecting ca. 8-9 scans. In the case of **7-N_3** the rapidity of photoreduction prevented collection of sufficient data for EXAFS analysis.

The software package EXAFSPAK[8] was employed for data reduction, averaging, and normalization.[9] The amplitude reduction factor S_0 was set to 0.9 and the coordination number N was fixed and varied iteratively. The remaining parameters, r, σ^2, and the edge shift parameter E_0, were allowed to freely float. Note that E_0 was linked for all shells, resulting in a single value. DFT energy-minimized structures were employed in conjunction with the software package FEFF 8.40[10] to calculate phase and amplitude parameters, which were fit in EXAFSPAK via the "opt" program. The quality of the fit was ascertained using the goodness-of-fit parameters F, defined as $F = \sum(\chi_{exptl} - \chi_{calc})^2$, and the F-factor, defined as $F = [\sum k^6(\chi_{exptl} - \chi_{calc})^2/\sum k^6 \chi_{exptl}^2]^{1/2}$. All pre-edge analyses were performed with the software package SSExafs[11] using previously reported methodology.[12]

The inclusion of four shells best reproduced the raw EXAFS data collected for **7** (Fit 33, Table S4). Examination of the Debye-Waller and F-factors associated with fits 1-7 indicate that a five-coordinate model best reproduces the raw EXAFS data. The bond length of 1.65 Å associated with the Fe–O/N scatterer is consistent with Fe(IV)–O_{oxo} bond distances previously

observed for other Fe(IV) species. Iterative fits of the Fe–O/N coordination number yielded a best fit of 0.8, corresponding with the relative amount of Fe(IV) in the sample. A second shell of Fe–N/O scatterers was introduced to model the nitrogen atoms deriving from TMG_2dien and $NCCH_3$. As DFT geometry optimization studies suggest that the axial Fe–N_{axial} bond elongates slightly (~ 2.15 Å) relative to Fe–$N_{TMG2dien}$ bonds in the equatorial plane, a third Fe–N/O shell was introduced to the fit. However, this either led to unreasonable values of σ^2 or resulted in excessively short (~ 1.8 Å) or long (~ 3.5 Å) optimized Fe–N/O bond lengths. Therefore, a single shell was used to model the N/O scatters at ~ 1.94 Å from the iron center, which presumably correspond to the supporting ligand and the bound acetonitrile. The inclusion of two shells of carbon scatterers, presumably associated with the TMG_2dien ligand, accurately reproduced the features observed at R ~ 2.4 and 2.9 Å in the Fourier-transformed data.

Similar to the fit obtained for **7**, the structural parameters of **7-Cl** are best fit with an Fe–O scatterer at 1.66 Å corresponding to the oxo moiety and three additional Fe–N/O at 1.94 Å attributed to the TMG_2dien ligand (Fit 19, Table S5). As for **7**, EXAFS cannot resolve the slight elongation of the axial Fe–$N_{TMG2dien}$ bond predicted by DFT. The spectroscopic perturbations upon substitution of chloride that were observed by UV-visible and Mössbauer spectroscopies are also reflected in the EXAFS data. A fifth chloride scatterer at 2.27 Å replaces the fourth N/O scatterer associated with **7**. The coordination numbers associated with both the O/N scatterer at 1.65 Å and the Cl scatterer were varied in units of 0.1, and *N* values of 0.8, roughly corresponding to the percentage of Fe(IV) in the sample, for both of these scatterers yielded chemically reasonable bond lengths, σ^2 parameters, and goodness-of-fit values.

Table S3. Pre-edge analysis parameters for **4**, **7**, **7-Cl**, and **7-N_3**.

Species	E_{edge} (eV)	$E_{pre\text{-}edge}$ (eV)	Height	Width	Area
4	7121.87	7112.66(9)	0.063(1)	2.09(4)	13.9(3)
		7114.57(7)	0.021(2)	0.70	1.6(1)
7	7123.556	7113.27(5)	0.105(1)	1.785(2)	19.9(3)
		7115.04(1)	0.022(2)	1.31	3.1(2)
7-Cl	7123.915	7113.928	0.109(2)	1.89(4)	21.9(6)
		7115.695	0.024(3)	0.81	2.1(2)
7-N_3	7124.155	7113.803	0.120(2)	1.94(4)	24.7(6)
		7115.659	0.043(2)	1.99	9.2(4)
		7118.051	0.035(2)	1.48	5.5(4)

Table S4. EXAFS fitting results for $[Fe(IV)(O)(TMG2dien)(MeCN)]^{2+}$ (**7**).

	Fe–O/N			Fe–N/O			Fe•••C			Fe•••C				*F*-
Fit	*N*	r (Å)	$\sigma^{2(a)}$	*N*	r (Å)	σ^2	*N*	r (Å)	σ^2	*N*	r (Å)	σ^2	F	Factor
1				4	1.9520	3.99							649.3	0.768
2				5	1.9500	5.68							721.2	0.809
3				6	1.9568	7.93							796.2	0.850
4	1	1.6444	8.50	2	1.9391	0.35							548.6	0.705
5	1	1.6475	5.42	3	1.9436	2.38							512.1	0.682
6	1	1.6504	3.95	4	1.9455	4.17							507.3	0.679
7	1	1.6512	2.97	5	1.9459	5.92							521.8	0.688
8	1	1.6439	4.40	2	1.9495	1.46							503.9	0.676
				2	1.9349	11.43								
9	1	1.6584	5.29	3	1.9443	2.00							503.1	0.676
				1	2.0630	3.85								
10	1	1.6567	5.01	2	1.9434	1.45							503.4	0.676
				2	1.9933	8.34								
11	1	1.5740	12.52	1	1.8727	-1.60							570.8	0.720
				3	2.1970	3.33								
12	1	1.6379	4.33	2	1.9568	1.27	2	2.8591	-1.90				380.0	0.587
				2	1.9194	13.02								
13	1	1.6360	4.26	2	1.9557	1.20	3	2.8578	-0.20				401.7	0.604
				2	1.9088	13.11								
14	1	1.6573	5.43	3	1.9478	2.34	3	2.8610	-0.10				404.0	0.606
				1	2.0599	7.69								
15	1	1.6574	5.11	3	1.9456	2.51	4	2.8608	1.35				427.3	0.623
				1	2.0419	8.42								
16	1	1.6566	4.79	3	1.9451	2.60	5	2.8616	2.83				450.4	0.639
				1	2.0307	9.17								
17	1	1.6393	2.35	3	1.9570	2.90	4	2.8495	4.92	1	3.3513	-5.70	269.9	0.495
				1	1.8493	3.45								
18	1	1.6521	4.64	3	1.9607	2.82	4	2.9198	2.02	2	3.0989	-3.30	290.2	0.513
				1	2.0813	7.68								
19	1	1.6522	4.57	3	1.9637	2.70	4	2.9179	1.06	3	3.0954	-2.00	294.7	0.517
				1	2.0973	6.74								
20	1	1.6453	2.92	3	1.9103	3.39	4	2.8481	3.88	4	3.3582	-1.20	230.1	0.457
				1	1.9964	0.34								
21	1	1.6335	3.29	3	1.9496	2.73	4	2.8466	3.47	5	3.3551	-0.30	226.0	0.453
				1	1.8366	6.90								
22	1	1.6482	3.72	4	1.9410	4.37	3	2.8483	1.61	6	3.3590	0.51	213.4	0.440
23	1	1.6481	3.60	4	1.9408	4.42	4	2.8492	3.50	6	3.3589	0.36	227.6	0.455
24	1	1.6312	3.18	2	1.9564	1.38	3	2.8465	1.18	7	3.3579	1.31	213.2	0.440
				2	1.8768	8.37								
25	1	1.6392	7.38	2	1.9375	0.61	3	2.8223	2.27	6	3.3531	0.64	237.7	0.465
				2	2.5354	10.76								
26	1	1.6442	4.84	3	1.9457	2.76	3	2.8501	2.33	6	3.3690	-1.20	199.2	0.425
				1	3.4995	-4.60								
27	1	1.6482	3.76	4	1.9399	4.33	3	2.8459	1.62	6	3.3597	0.50	214.0	0.441
28	1	1.6488	3.86	4	1.9416	4.31	3	2.8490	1.27	8	3.3610	1.86	219.2	0.446
29	0.9	1.6474	3.14	4	1.9419	4.48	3	2.8490	1.64	6	3.3596	0.50	215.3	0.442
30	0.8	1.6468	2.53	4	1.9430	4.59	3	2.8498	1.66	6	3.3602	0.49	218.1	0.445
31	0.8	1.6469	2.41	4	1.9428	4.65	4	2.8509	3.59	6	3.3601	0.33	232.2	0.459
32	0.8	1.6470	2.62	4	1.9432	4.55	3	2.8501	1.47	7	3.3611	1.18	220.4	0.447
33	**0.8**	**1.6471**	**2.48**	**4**	**1.9431**	**4.61**	**4**	**2.8508**	**3.35**	**7**	**3.3610**	**1.02**	**235.7**	**0.463**

[a]Fourier-transform range is 2 – 14 $Å^{-1}$ (resolution = 0.13 Å), and σ^2 is in units of 10^3 $Å^2$.

Table S5. EXAFS fitting results for $[Fe(IV)(O)(TMG2dien)(Cl)]^+$ (**7-Cl**).

	Fe–N/O			Fe–O/N			Fe–Cl			Fe•••C			Fe•••C/N				*F*-
Fit	*N*	r (Å)	$\sigma^{2(a)}$	*N*	r (Å)	σ^2	*N*	r (Å)	σ^2	*N*	r (Å)	σ^2	*N*	r (Å)	σ^2	F	factor
1	2	1.942	0.00	1	1.672	5.44	1	2.242	7.76							382.0	0.690
2	3	1.942	2.85	1	1.663	3.15	1	2.267	7.79							381.2	0.689
3	4	1.941	5.41	1	1.657	1.97	1	2.283	8.06							390.0	0.697
4	3	1.945	3.05	0.9	1.662	2.52	0.9	2.272	6.94							380.2	0.688
5	3	1.948	3.30	0.8	1.661	1.85	0.8	2.279	6.03							379.4	0.687
6	3	1.952	3.19	0.8	1.663	1.89	0.8	2.286	5.43	2	2.929	3.77				342.1	0.653
7	3	1.953	3.24	0.8	1.664	1.94	0.8	2.289	5.33	3	2.938	5.51				333.5	0.644
8	3	1.940	3.36	0.8	1.658	0.98	0.9	2.269	5.72	3	2.923	2.86	3	3.384	-2.30	222.2	0.526
9	3	1.939	3.38	0.9	1.657	1.00	0.8	2.267	5.93	3	2.918	3.22	4	3.382	-0.90	220.6	0.524
10	3	1.939	3.38	0.8	1.657	1.04	0.8	2.266	6.10	3	2.915	3.59	5	3.381	0.29	220.8	0.524
11	3	1.938	3.39	0.8	1.657	1.08	0.8	2.265	6.27	3	2.912	3.91	6	3.380	1.34	222.4	0.526
12	3	1.937	3.39	0.8	1.657	1.10	0.8	2.264	6.41	3	2.909	4.31	7	3.379	2.32	224.8	0.529
13	3	1.939	3.44	0.8	1.657	1.10	0.8	2.267	6.24	3	2.914	3.89	6	3.379	1.37	222.2	0.526
14	3	1.944	3.49	0.8	1.658	1.26	0.8	2.274	6.04	4	2.924	6.35	6	3.385	1.63	222.9	0.527
15	3	1.943	3.49	0.8	1.658	1.30	0.8	2.273	6.15	4	2.923	6.88	7	3.383	2.65	225.7	0.530
16	2	1.961	-0.60	1	1.686	7.78	1	2.209	12.16							385.6	0.693
	1	2.154	0.05														
17	2	1.957	-0.60	1	1.687	6.82	1	2.251	9.18	3	2.946	5.18				335.2	0.646
	1	2.148	3.97														
18	2	1.937	0.26	1	1.666	3.94	1	2.244	7.84	3	2.911	3.52	6	3.379	1.37	222.3	0.5261
	1	1.966	27.78														
19	**3**	**1.939**	**3.39**	**0.8**	**1.657**	**1.11**	**0.8**	**2.266**	**6.21**	**3**	**2.913**	**3.96**	**6**	**3.380**	**1.38**	**222.2**	**0.526**

[a]Fourier-transform range is 2 – 12 $Å^{-1}$ (resolution = 0.158 Å), and σ^2 is in units of 10^3 $Å^2$.

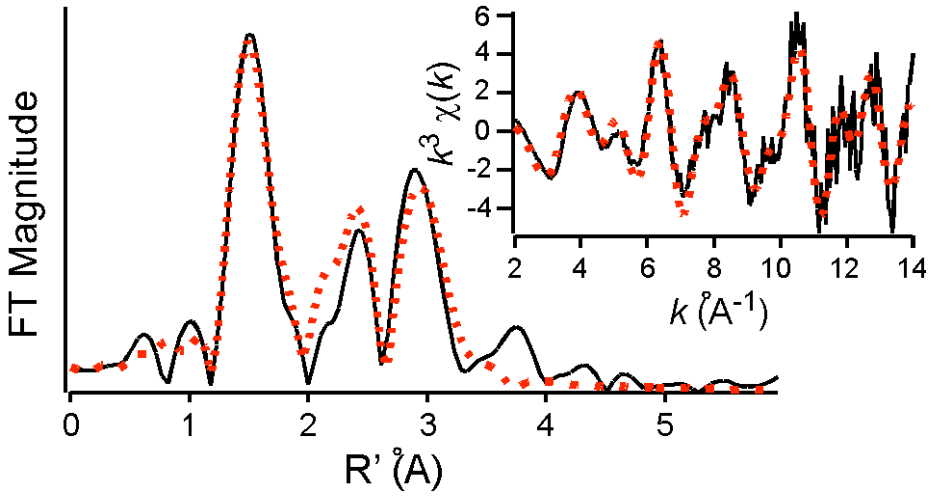

Figure S11. Fe K-edge unfiltered EXAFS data ($k^3\chi(k)$, inset) and the corresponding Fourier transform for **7**. The red dots and solid black lines correspond to the experimental data and fits, respectively.

DFT calculations.

DFT calculations were performed using Becke's three parameter hybrid (B3LYP) functional and basis set 6-311G provided by Gaussian'03 software package.[13] The quadrupole splitting ΔE_Q was calculated using the property keyword of the Gaussian code and Q(^{57}Fe) = 0.17 barn. The ^{57}Fe isomer shift δ was evaluated from the DFT charge density at the Fe nucleus using the calibration given by Vrajmasu et al.[14] The SCF procedure and geometry optimization were terminated upon reaching the default convergence criteria. The populations were calculated with the population keyword. The initial structural model for **7**, **7-N$_3$** and **7-Cl** were constructed using the crystal structure of **2** and replacing the two triflate ligands by an oxygen atom at the axial position and an X ligand (X = $NCCH_3$ for **7**, N_3^- for **7-N$_3$**, and Cl^- for **7-Cl**) at the equatorial position.

Table S6. Spectroscopic parameters of selected oxoiron(IV) complexes.

Complex	D [cm^{-1}]	E/D	$A_{x,y,z}/g_n\beta_n$ (T)[e]	ΔE_Q [mm s^{-1}]	η	δ [mm s^{-1}]
7 (exp)	4.6[a] 4.2[b]	0.09[a] 0.10[b]	-13.9, -15.8, -26.0	0.58[c]	0.20	0.08
7 (DFT)	-	-	-12.7, -16.5, -26.5[e]	1.17	0.55	0.13
7-N$_3$ (exp)	4.6[a] 5.0[b]	0.04[a] 0.05[b]	-15.5, -14.5, -27.0	-0.30[d]	0.35	0.11
7-N$_3$ (DFT)	-	-	-15.9, -14.7, -26.5[e]	-0.26	0.28	0.12
7-Cl (exp)	4.1[a] 4.2[b]	0.13[a] 0.14[b]	-15.1, -15.4, -26.6	0.41	0.53	0.08
7-Cl (DFT)	-	-	-13.9, 16.3 -26.9	0.74	0.23	0.11

[a] Determined by Mössbauer; [b] Determined by EPR; [c] The electric field gradient (EFG) tensor and the A-tensor are rotated relative to the ZFS tensor by α_{EFG} = 50°, β_{EFG} = 45° and by α_A = 55° (WMOSS convention); see the Mössbauer comments above; [d] the EFG tensor and the A-tensor are rotated by α_{EFG} = 30°, β_{EFG} = 60° and by α_A = 20°; [e] Calculated A-tensors were obtained by taking the experimentally determined A_{iso} and adding the spin-dipolar term obtained from DFT.

Table S7. Electronic energies of the lowest excited spin states (S = 1 and S = 0) for **7**, **7**-N_3 and **7**-Cl calculated by DFT.[a,b]

	S = 2	S = 1	S = 0
7	0	6	13
7-N_3	0	7	12
7-Cl	0	7	10

[a] The ground state energy is set to zero. [b] Unit: $10^3 cm^{-1}$.

Figure S12. Ball-and-stick models of the DFT geometry optimized structures of (**A**) **7**, (**B**) **7-N_3** and (**C**) **7-Cl**. Hydrogen atoms have been omitted for clarity. Atom color scheme: C, gray; Cl, green; Fe, magenta; N, blue; O, red.

Table S8. Selected bond lengths and angles of **7**, **7**-N_3 and **7**-Cl calculated by DFT.

Selected bond lengths (Å) and angles (°)	**7** (X = CH_3CN)	**7-N_3** (X = N_3^-)	**7-Cl** (X = Cl^-)
Fe-X	2.1433	1.9224	2.3498
Fe-O	1.6485	1.6489	1.6444
Fe-N_{eq}(1)	1.9618	2.0346	1.9934
Fe-N_{eq}(2)	1.9654	2.0287	1.9908
Fe-N_{ax}	2.1497	2.2089	2.2124
O-Fe-N_{ax}	177.72	174.23	171.84
O-Fe-X	90.61	96.54	95.88
O-Fe-N_{eq}(1)	95.81	95.96	95.51
O-Fe-N_{eq}(2)	95.11	95.07	93.05
N_{ax}-Fe-X	91.66	89.23	92.28
N_{ax}-Fe-N_{eq}(1)	83.72	81.91	82.77
N_{ax}-Fe-N_{eq}(2)	83.55	81.63	81.73
X-Fe-N_{eq}(1)	108.59	110.67	104.24
X-Fe-N_{eq}(2)	119.58	124.42	127.06
N_{eq}(1)-Fe-N_{eq}(2)	130.331	121.82	126.65

Table S9. Iron 3d orbital population and spin population of **7**, **7-N_3**, **7-Cl** and **2**.

		d_{xz}	d_{yz}	d_{x2-y2}	d_{xy}	d_{z2}	Total	Fe Charge
7	Population	1.39	1.41	1.15	1.16	0.94	6.05	1.57
	Spin Population	0.60	0.59	0.82	0.81	0.21	3.03	
7-N_3	Population	1.33	1.37	1.19	1.19	0.96	6.04	1.56
	Spin Population	0.66	0.62	0.79	0.79	0.21	3.07	
7-Cl	Population	1.37	1.39	1.19	1.15	0.96	6.06	1.46
	Spin Population	0.63	0.60	0.79	0.83	0.20	3.05	
2[a]	Population	1.38	1.37	1.16	1.16	0.93	6.00	1.64
	Spin Population	0.61	0.61	0.82	0.82	0.18	3.04	

[a] Values reported in reference 15.

Table S10. Oxo 2p orbital population and spin population of **7**, **7-N_3**, **7-Cl** and **2**.

		p_{xs}	p_y	p_z	Total	O Charge
7	Population	1.56	1.55	1.38	4.49	-0.45
	Spin Population	0.39	0.40	-0.09	0.7	
7-N_3	Population	1.62	1.59	1.35	4.56	-0.51
	Spin Population	0.32	0.36	-0.13	0.55	
7-Cl	Population	1.61	1.56	1.34	4.51	-0.46
	Spin Population	0.34	0.39	-0.12	0.61	
2	Population	1.58	1.58	1.37	4.53	-0.48
	Spin Population	0.37	0.37	-0.11	0.63	

Table S11. Cartesian coordinates (Å) for the DFT energy minimized model of **7**.

		x	y	z
1	Fe	0.046962	0.509248	0.035891
2	N	1.711588	-0.32653	0.651473
3	N	0.176925	1.584175	1.892972
4	N	-1.8119	0.206214	0.597533
5	N	3.835753	-1.04914	-0.13787
6	N	1.934993	-2.33374	-0.57813
7	N	-3.65105	-1.30093	0.45975
8	N	-3.04039	-0.03407	-1.4043
9	C	2.235262	0.222735	1.936745
10	C	1.031462	0.675909	2.748988
11	C	-1.23346	1.69732	2.423105
12	C	-2.02488	0.455603	2.052883
13	C	2.488205	-1.22872	-0.02989
14	C	4.444747	0.28993	-0.22665
15	C	4.79574	-2.17462	-0.16116
16	C	2.40721	-2.91297	-1.85343
17	C	0.722231	-2.9637	-0.0323
18	C	0.792593	2.953844	1.840475
19	C	-2.81868	-0.38191	-0.11499
20	C	-3.18145	-2.28279	1.454203
21	C	-5.09284	-1.38159	0.136072
22	C	-3.52567	-0.99929	-2.41245
23	C	-2.68664	1.286592	-1.94526
24	O	-0.07531	-0.36697	-1.35514
25	H	2.924699	1.055069	1.783148
26	H	2.782539	-0.54698	2.483847
27	H	0.433376	-0.18832	3.031323
28	H	1.331149	1.197833	3.66076
29	H	-1.68145	2.571411	1.954411
30	H	-1.21723	1.859974	3.503948
31	H	-1.70892	-0.39589	2.659283
32	H	-3.08309	0.617675	2.262888
33	H	3.681245	1.030656	-0.44431
34	H	5.170918	0.29181	-1.03943
35	H	4.964548	0.556851	0.695208
36	H	4.30683	-3.08841	0.160642
37	H	5.605702	-1.95143	0.532803
38	H	5.222417	-2.32345	-1.15336
39	H	3.124017	-2.2498	-2.32567
40	H	1.549225	-3.01854	-2.51642

41	H	2.860649	-3.89308	-1.70584
42	H	0.537282	-2.59301	0.970669
43	H	0.879623	-4.0416	0.011192
44	H	-0.13608	-2.74891	-0.66611
45	H	0.829146	3.383368	2.843793
46	H	0.195887	3.596079	1.201436
47	H	1.800403	2.901797	1.440815
48	H	-2.0968	-2.32992	1.450337
49	H	-3.56791	-3.26573	1.184705
50	H	-3.53351	-2.04262	2.458766
51	H	-5.40514	-0.49323	-0.40368
52	H	-5.65384	-1.435	1.068911
53	H	-5.32694	-2.26559	-0.45789
54	H	-3.51323	-2.00508	-2.00683
55	H	-2.85445	-0.96435	-3.27
56	H	-4.53433	-0.75599	-2.7467
57	H	-2.50384	1.980998	-1.13207
58	H	-3.52077	1.653653	-2.54353
59	H	-1.80046	1.216883	-2.57407
60	N	0.539576	2.266742	-1.08762
61	C	0.807149	3.067311	-1.88582
62	C	1.136554	4.062224	-2.88964
63	H	0.262453	4.670782	-3.12666
64	H	1.926841	4.724554	-2.53386
65	H	1.476751	3.578561	-3.80643

Table S12. Cartesian coordinates (Å) for the DFT energy minimized model of **7-N_3**.

		x	y	z
1	Fe	-0.071466	0.599145	0.277546
2	N	-1.745939	0.026538	-0.726411
3	N	-0.156881	2.270895	-1.163787
4	N	1.780274	0.392188	-0.524907
5	N	-3.872357	-0.886238	-0.170706
6	N	-1.991911	-2.271128	-0.299066
7	N	3.612935	-1.071849	-0.931181
8	N	3.021666	-0.513236	1.259978
9	C	-2.305590	1.117168	-1.562313
10	C	-1.122697	1.810186	-2.224535
11	C	1.236499	2.436102	-1.705289
12	C	1.924915	1.083976	-1.828000
13	C	-2.524574	-1.023333	-0.397207
14	C	-4.422493	0.304624	0.497080

15	C	-4.853476	-1.919398	-0.542726
16	C	-2.405327	-3.220769	0.749486
17	C	-0.773535	-2.648513	-1.024408
18	C	-0.617821	3.572414	-0.579155
19	C	2.778413	-0.389091	-0.071936
20	C	3.122754	-1.679190	-2.176507
21	C	5.051930	-1.242717	-0.666215
22	C	3.448644	-1.788089	1.862985
23	C	2.676708	0.532673	2.234417
24	O	0.029012	-0.746934	1.224703
25	H	-2.879442	1.840425	-0.979097
26	H	-2.976751	0.714558	-2.324937
27	H	-0.610760	1.101477	-2.872729
28	H	-1.442761	2.662293	-2.831448
29	H	1.782481	3.054539	-0.995354
30	H	1.211157	2.960583	-2.666184
31	H	1.482784	0.505370	-2.643926
32	H	2.977585	1.232408	-2.078343
33	H	-3.620632	0.873336	0.958935
34	H	-5.109411	-0.015985	1.281508
35	H	-4.971127	0.944979	-0.197392
36	H	-4.384514	-2.663136	-1.179855
37	H	-5.669199	-1.450999	-1.095631
38	H	-5.274670	-2.416164	0.333791
39	H	-3.141116	-2.762931	1.401973
40	H	-1.532346	-3.476377	1.350713
41	H	-2.821398	-4.132805	0.318534
42	H	-0.622946	-1.964898	-1.854143
43	H	-0.893924	-3.662537	-1.408900
44	H	0.091179	-2.607086	-0.363445
45	H	-0.576575	4.356515	-1.340790
46	H	0.010670	3.829835	0.265341
47	H	-1.631130	3.476679	-0.205654
48	H	2.037494	-1.714306	-2.170023
49	H	3.498032	-2.701719	-2.245952
50	H	3.459292	-1.132812	-3.060756
51	H	5.354667	-0.605109	0.158627
52	H	5.614659	-0.951677	-1.554771
53	H	5.302755	-2.278004	-0.425078
54	H	3.464002	-2.573235	1.114246
55	H	2.731378	-2.061989	2.637121
56	H	4.437867	-1.702782	2.315880
57	H	2.460516	1.462178	1.720235

58	H	3.527235	0.682263	2.901471
59	H	1.810143	0.239244	2.823842
60	N	-0.513073	1.827486	1.688802
61	N	-0.634451	1.598454	2.896593
62	N	-0.751018	1.435363	4.042729

Table S13. Cartesian coordinates (Å) for the DFT energy minimized model of **7-Cl**.

		x	y	z
1	Fe	-0.058514	0.498375	0.369286
2	N	-1.755387	0.105180	-0.600195
3	N	-0.139793	2.363600	-0.817711
4	N	1.782781	0.438169	-0.385366
5	N	-3.861818	-0.809888	0.017994
6	N	-2.065447	-2.221620	-0.484329
7	N	3.626641	-0.977805	-0.890108
8	N	3.022693	-0.578296	1.334048
9	C	-2.324446	1.304113	-1.265066
10	H	-2.849197	1.959854	-0.567250
11	H	-3.040584	1.011238	-2.036155
12	C	-1.151945	2.044334	-1.892321
13	H	-0.678441	1.404405	-2.635065
14	H	-1.471644	2.966667	-2.385099
15	C	1.239290	2.566435	-1.389890
16	H	1.810715	3.126371	-0.652303
17	H	1.183789	3.164475	-2.304792
18	C	1.915361	1.226324	-1.633430
19	H	1.455858	0.713041	-2.483042
20	H	2.965548	1.385189	-1.885859
21	C	-2.553085	-0.960938	-0.351283
22	C	-4.297112	0.304138	0.881446
23	H	-3.436953	0.777474	1.346340
24	H	-4.931019	-0.096307	1.673205
25	H	-4.873157	1.044514	0.322261
26	C	-4.918628	-1.753889	-0.385725
27	H	-4.553917	-2.406242	-1.173524
28	H	-5.767855	-1.186138	-0.767860
29	H	-5.263043	-2.363211	0.451966
30	C	-2.434616	-3.308425	0.440904
31	H	-3.060491	-2.923205	1.238598
32	H	-1.523271	-3.705227	0.888140
33	H	-2.957835	-4.114102	-0.076376
34	C	-0.934157	-2.521996	-1.370558

35	H	-0.830711	-1.729627	-2.105277
36	H	-1.129625	-3.465047	-1.882818
37	H	-0.012336	-2.601922	-0.795604
38	C	-0.550270	3.619556	-0.101275
39	H	-0.503300	4.464924	-0.793886
40	H	0.108307	3.791514	0.742278
41	H	-1.556401	3.521332	0.288687
42	C	2.788983	-0.367359	0.015211
43	C	3.137706	-1.501722	-2.174145
44	H	2.052920	-1.552295	-2.165383
45	H	3.525643	-2.511626	-2.316311
46	H	3.463507	-0.889638	-3.018325
47	C	5.067472	-1.156191	-0.638423
48	H	5.366171	-0.576117	0.229218
49	H	5.626419	-0.798459	-1.504594
50	H	5.326023	-2.203854	-0.471698
51	C	3.474444	-1.882465	1.851932
52	H	3.483912	-2.621776	1.057766
53	H	2.772063	-2.209182	2.618550
54	H	4.469511	-1.812633	2.294002
55	C	2.637972	0.391159	2.374787
56	H	2.472122	1.366090	1.929921
57	H	3.451961	0.463889	3.096878
58	H	1.728958	0.082452	2.886569
59	O	0.079596	-0.989563	1.055587
60	Cl	-0.752268	1.601653	2.324553

Substrate Oxidation Kinetics.

Solutions of **7** were prepared by adding 1 equivalent of 2-(^{t}BuSO$_2$)C$_6$H$_4$IO dissolved in a small amount of dichloromethane to 2 mL of 0.2-0.1 mM CH_3CN solutions of **5** prepared under an inert atmosphere. Kinetic measurements of substrate oxidations were performed at -30° C and monitored by the formation and decay of appropriate bands in their UV-Vis absorbance spectra (Figures S13 and S14). Fitting to the resultant decay and growth curves obtained from the spectra yielded pseudo-first order rate constants, k_{obs}, that were found in all cases to be strictly first order in substrate (Figure S15). The measurements of k_{obs} values for the substrate oxidations were repeated on subsequent days with different concentrations of **7** to ensure reproducibility.

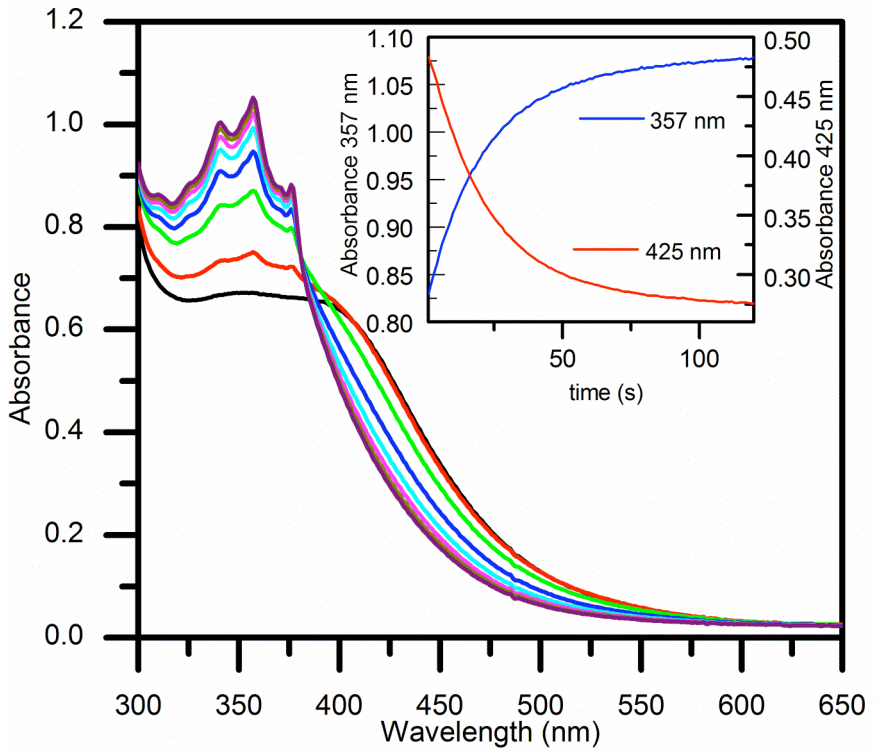

Figure S13. Typical UV-Vis changes seen upon reaction of **7** with 9,10-dihydroanthracene. The reaction was monitored by the decay of the shoulder attributed to **7** at 425 nm and the formation of the anthracene product band at 357 nm. In all cases, the pseudo-first order rate constants obtained from monitoring the the 357 and 425 nm absorbances were nearly identical.

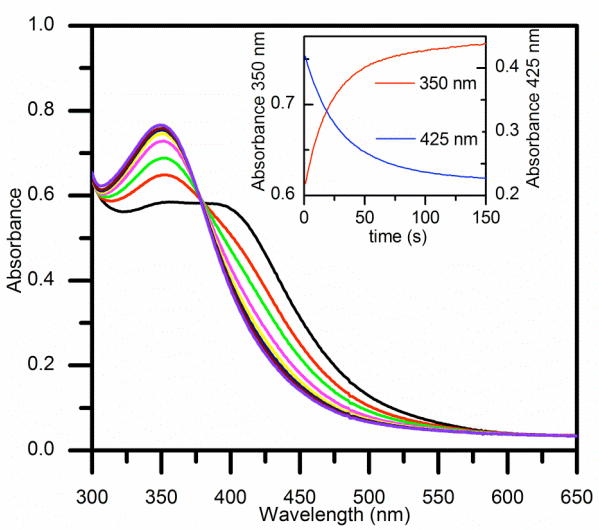

Figure S14. Typical UV-Vis changes seen upon reaction of **7** with 1,4-cyclohexadiene. The reaction was monitored by the decay of the shoulder attributed to **7** at 425 nm and the formation of the decay product band at 350 nm. In all cases, the pseudo-first order rate constants obtained from monitoring the 350 and 425 nm absorbances were nearly identical.

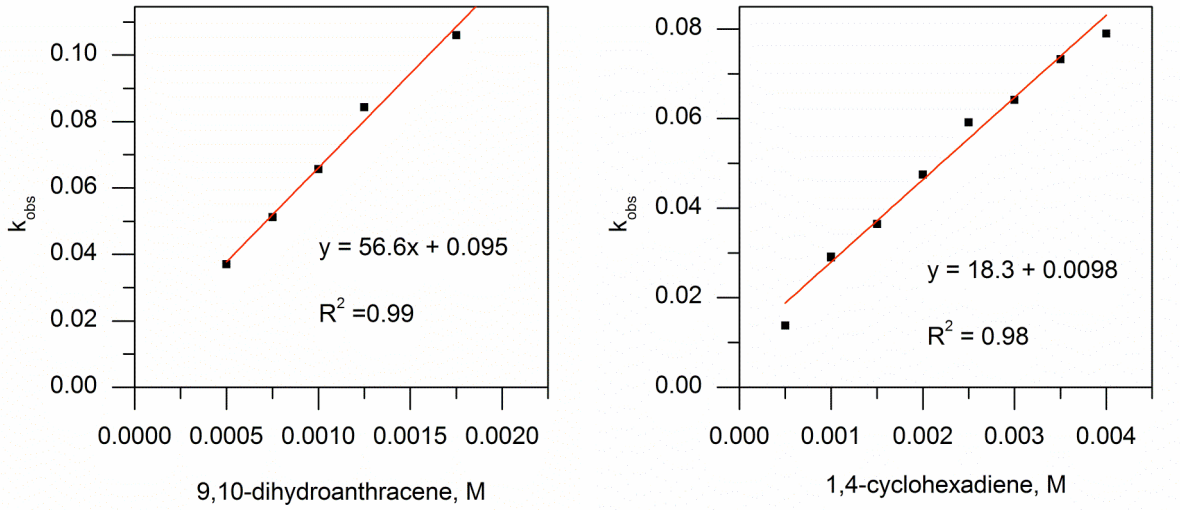

Figure S15. Plots of k_{obs} *vs.* substrate concentration obtained from reaction of **7** with 9,10-dihydroanthracene (DHA, left) and 1,4-cyclohexadiene (CHD, right). Linear fits yielded second order rate constants, k_2, of 57 and 18 $M^{-1}s^{-1}$, respectively.

References.

(1) Macikenas, D.; Skrzypczak-Jankun, E.; Protasiewicz, J. D. *J. Am. Chem. Soc.* **1999**, *121*, 7164-7165.

(2) Hagadorn, J. R.; Que, L.; Tolman, W. B. *Inorg. Chem.* **2000**, *39*, 6086-6090.

(3) Wittmann, H.; Raab, V.; Schorm, A.; Plackmeyer, J.; Sundermeyer, J. *Eur. J. Inorg. Chem.* **2001**, 1937-1948.

(4) Herres-Pawlis, S.; Neuba, A.; Seewald, O.; Seshadri, T.; Egold, H.; Flörke, U.; Henkel, G. *Eur. J. Org. Chem.* **2005**, *2005*, 4879-4890.

(5) Blessing, R. H. *Acta Crystallogr., Sect. A: Found. Crystallogr.* **1995**, *A51*, 33-8.

(6) *SAINT+ V 6.45*; Bruker Analytical X-Ray Systems: Madison, WI 2003.

(7) *SHELXTL V 6.14*; Bruker Analytical X-Ray Systems: Madison, WI 2000.

(8) George, G. N.; Stanford Synchrotron Radiation Laboratory, Stanford Linear Accelerator Center: Stanford, CA, 2000.

(9) Klinker, E. J.; Jackson, T. A.; Jensen, M. P.; Stubna, A.; Juhasz, G.; Bominaar, E. L.; Münck, E.; Que, L. *Angew. Chem. Int. Ed.* **2006**, *45*, 7394-7397.

(10) Ankudinov, A. L.; Ravel, B.; Rehr, J. J.; Conradson, S. D. *Phys. Rev. B* **1998**, *58*, 7565-7576.

(11) Scarrow, R. C.; Trimitsis, M. G.; Buck, C. P.; Grove, G. N.; Cowling, R. A.; Nelson, M. J. *Biochemistry* **1994**, *33*, 15023-15035.

(12) Rohde, J.-U.; Torelli, S.; Shan, X.; Lim, M. H.; Klinker, E. J.; Kaizer, J.; Chen, K.; Nam, W.; Que, L. *J. Am. Chem. Soc.* **2004**, *126*, 16750-16761.

(13) Gaussian 03, Revision E.01, M. J. Frisch, G. W. Trucks, H. B. Schlegel, G. E. Scuseria, M. A. Robb, J. R. Cheeseman, J. A. Montgomery, Jr., T. Vreven, K. N. Kudin, J. C. Burant, J. M. Millam, S. S. Iyengar, J. Tomasi, V. Barone, B. Mennucci, M. Cossi, G. Scalmani, N. Rega, G. A. Petersson, H. Nakatsuji, M. Hada, M. Ehara, K. Toyota, R. Fukuda, J. Hasegawa, M. Ishida, T. Nakajima, Y. Honda, O. Kitao, H. Nakai, M. Klene, X. Li, J. E. Knox, H. P. Hratchian, J. B. Cross, V. Bakken, C. Adamo, J. Jaramillo, R. Gomperts, R. E. Stratmann, O. Yazyev, A. J. Austin, R. Cammi, C. Pomelli, J. W. Ochterski, P. Y. Ayala, K. Morokuma, G. A. Voth, P. Salvador, J. J. Dannenberg, V. G. Zakrzewski, S. Dapprich, A. D. Daniels, M. C. Strain, O. Farkas, D. K. Malick, A. D. Rabuck, K. Raghavachari, J. B. Foresman, J. V. Ortiz, Q. Cui, A. G. Baboul, S. Clifford, J. Cioslowski, B. B. Stefanov, G. Liu, A. Liashenko, P. Piskorz, I. Komaromi, R. L. Martin, D. J. Fox, T. Keith, M. A. Al-Laham, C. Y. Peng, A. Nanayakkara, M. Challacombe, P. M. W. Gill, B. Johnson, W. Chen, M. W. Wong, C. Gonzalez, and J. A. Pople, Gaussian, Inc., Wallingford CT, **2004**.

(14) Vrajmasu, V.; Münck, E.; Bominaar, E. L. *Inorg. Chem.* **2003**, *42*, 5974-5988.

(15) England, J.; Martinho, M.; Farquhar, E. R.; Frisch, J. R.; Bominaar, E. L.; Münck, E.; Que, L., Jr. *Angew. Chem., Int. Ed.* **2009**, *48*, 3622-3626.